Construction and Building Materials 165 (2018) 898–913

Contents lists available at ScienceDirect

Construction and Building Materials

journal homepage: www.elsevier.com/locate/conbuildmat

Impact of the height imperfections of masonry blocks on the load bearing capacity of dry-stack masonry walls

Gelen Gael Chewe Ngapeya *, Danièle Waldmann, Franck Scholzen

Université du Luxembourg, Luxembourg

HIGHLIGHTS

- Analysis of the load bearing capacity of dry-stacked bocks with height imperfections.
- Determination of multiplier coefficient for stress intensity due to imperfections.
- Imperfection governs actual contact, load percolation and bearing capacity.
- Definition of five different load cases for the blocks in a wall.
- Comparison of analytical approach to FE analysis of the multiplier coefficient.

ARTICLE INFO

Article history:
Received 21 July 2017
Received in revised form 23 November 2017
Accepted 27 December 2017

Keywords:
Dry-stacked masonry block
Load percolation
Height imperfections of masonry block
Load case
Actual contact

ABSTRACT

Dry-stacked masonry walls gives rise to geometric imperfections: the height variation of different masonry blocks ΔH and the roughness of the support area Δh. This paper studies the effect of ΔH on the structural response and the load bearing capacity of masonry walls by highlighting the load percolation. Furthermore, an algorithm was developed to define a stress multiplier coefficient respecting the imperfections ΔH. The algorithm allowed predicting 77% of the amplified stress compared to the FE analysis and showed that the geometric imperfections govern the load percolation in a wall as well as the cracking mode and the bearing capacity.

1. Introduction

The masonry block is one of the oldest construction elements, commonly and traditionally used for centuries around the world. It can be classified in different product families according to the nature of its constitutive materials, its internal structure [1] (full or hollow blocks, blocks with cells, etc.), its field of application, its mode of installation (with joints or dry-stacked) and its contribution to the stability of the superstructure. Moreover, a masonry block is also characterised by its dimensions, its mechanical, thermal and acoustic properties. Many historical and old constructions built with mortar joints have presented a significant loss of wall performances due to physical, chemical and mechanical degradation of the mortar layer [2]. In addition to these defects, the optimization of the construction times and the limitation of imperfections in the walls led to the development of dry stacking masonry block systems.

As outlined by former authors [3–5], the load bearing behaviour of the masonry blocks with mortar layer is widely different from the behaviour of the mortarless masonry blocks in many viewpoints. Firstly, Gihad Mohamad et al. [3] carried out experimental research on the mechanics of hollow concrete masonry walls under compression. One of its key conclusions was that the mortar layer is highly responsible for the nonlinear behaviour of the wall. He also contradicts the absolute linear relationship between elasticity modulus of the block and the compressive strength described by Eurocode 6 [1]. More recently, the same author [6] showed that for the grouted masonry wall, the mortar layer mostly governs the masonry failure process. For masonry blocks stacked with weak mortars, failure starts with mortar crushing which leads to a localized tensile stresses in the masonry blocks. However, for masonry blocks stacked with a better mortar, cracking starts later and grow until reaching the mortar layer. Secondly, Fahmy [7] highlighted that, in vertical and horizontal direction, the mortar

* Corresponding author.
E-mail addresses: gael.chewengapeya@uni.lu (G.G. Chewe Ngapeya), daniele.waldmann@uni.lu (D. Waldmann), franck.scholzen@uni.lu (F. Scholzen).

https://doi.org/10.1016/j.conbuildmat.2017.12.183
0950-0618/

layer between the different blocks increases the strength of cohesion among them.

Taking into account that full-scale experimental tests are expensive, finite element analysis has been used in many studies to predict the in-service and near-collapse behaviour of such complex structures with sufficient reliability. Former researchers have led investigations on numerical modelling of masonry blocks, especially for the investigation of the behaviour of masonry walls with the mortar layer. However, whatever the case, for FEM analysis two different approaches can be used: the micro-model approach, which use individual properties of the constituent materials and their interfaces separately [4,5,8,9], and the macro-model approach, which for its part uses homogenised properties for the blocks and the mortar [10–12]. The micro-model provides a good insight on the behaviour of each constituent (masonry block, mortar layer, contact areas) separately described by means of specific constitutive equations. This method leads to the most accurate prediction, whilst, the macro-model approach needs less computational effort and thus allows an analysis of high structure in short time.

In their outcomes, Waleed et al. [4,5] propose a finite element model to analyse the interlocking mortarless hollow concrete block system subjected to axial compression loads. Based on the experimental tests, they described the actual contact of dry joint while taking into account the local imperfection and the normal stress in a masonry block. To predict the load carrying capacity and the failure mechanism of their masonry block, they have implemented the developed stress-deformation behaviour of the masonry block in a finite element program. Given that the state of contact between the joints varies nonlinearly, they executed their program with small load increments of loading in a way to follow the nonlinear behaviour of the joint. However, they performed the numerical analysis on a 2D model, thereby removing the possibility to assess cracks occurring out of the plane. Zucchini et al. [10] and Bati et al. [13] have proposed to apply the homogenisation techniques developed by Bakhvalov and Panasenko [14] to analyse the behaviour of mortar masonry structures. The developed homogenisation approach consists on describing the behaviour of the composite masonry walls in terms of macro-strains and stresses so that the composite structure can be assumed as homogeneous. The composite structure built up of basic cells (masonry blocks, vertical and horizontal joint layers) is transposed to a homogeneous structure whose stresses and strains in the loading plane are analytically expressed in function of the geometric dimensions, the stresses and strains of the basic cells. Indeed, the elastic response of the basic cells to a generic load is determined by the study of six basic loading conditions. Furthermore, the Poisson's ratio and the Young's modulus of the equivalent orthotropic homogeneous material are derived from the elastic strains of the basic cell loaded with a uniform normal stress on the two faces perpendicular to the loading plane.

The outcomes of the homogenisation approach showed that up to a stiffness ratio of one thousand between masonry block and mortar layer, the maximum error in the calculation of the homogenised Young's modulus is lower than five percent compared to the Young's modulus obtained by finite element analysis of the heterogeneous structure. However, Anthoine [11,12] has shown that the standard homogenisation technique does not take into account the different bond patterns (tenon and mortise, solid seal, etc.). In further researches, Zucchini and Lourenço [15] deeply enhance their homogenisation approach by a micro mechanical modelling and they reached to three conclusions. Firstly, during the compressive loading of the grouted masonry, the nonlinear deformation of the mortar starts very early for the weak mortars, whereas the first cracking of the masonry block begins later. For this configuration, the masonry block is under compression in the loading direction and under tension in the two other directions, while the mortar layer is in a tri-axial compression state because of the lateral confinement. Secondly, they highlighted that when the mortar is stiffer but still weaker in compression than the masonry block, the masonry block does not fail by reaching the tensile strength limit, but by reaching the compression strength of its partitions. Finally, when the mortar is much stiffer and stronger than the masonry block, the nonlinear deformation starts earlier in the masonry block than in the mortar layer. In this case the masonry block reaches failure by crushing of its face shells.

Prior to the outcomes of these former authors [2–4,6,7,10,15,16], McNary and Abrams [17] had already highlighted that under a normal compression, a softer mortar increases the tensile stress in the block in the perpendicular direction to the loading, which then decreases the stiffness of the masonry block. As Adrien Costigan et al. [18], McNary and Abrams also noted that the stress–strain relationship of bounded masonry blocks becomes increasingly non-linear as the mortar strength lowers. Anastasios Drougkas et al. [9] focused on the numerical prediction of the compressive response of a masonry block, its failure mode, its hardening and softening behaviour under compression by means of finite element micro-modelling techniques. Based on a panel of fifty former experimental tests, they showed that a three-dimensional micro-model allows a more accurate and general simulation of the compressive behaviour of a masonry block. Nevertheless, Salah's [16] results on the prediction of the compressive strength of a masonry block showed that most numerical codes underestimate the compressive strength of the ungrouted masonry block with high coefficients of variation. Based on statistical analysis of 248 experimental datasets, they fixed the underestimation at 82% of the compressive strength of the hollow concrete masonry block.

As it can be seen, although some work has been done on dry-stacked masonry [4,5], most experimental and numerical research are focused on grouted masonry. Nevertheless, mortar-less masonry block is full of great advantages among others: the speed of wall construction (faster aligned), the ease of deconstruction, the possibility to reuse the masonry blocks, the flexibility, the elimination of the mortar quality variation and the possibility to construct during cold time. Despite all those advantages, it is worth to stress out that there are two major disadvantages linked to the dry-stacked masonry blocks [19,20]: the height imperfection of the masonry blocks due to the production process and the roughness of the contact area. Agaajani [20] observed that within a panel of manufactured blocks, the final block height follows a statistical distribution of a Gauss curve, thereby causing an undoubted height variation when blocks are aligned in a course. Indeed, in the production process, wear and tolerances of formworks manufacturing lead to the production of blocks with a height variation of ±2 mm. To this may be added the effect of shrinkage. These geometrical imperfections create stress concentration in the blocks and thus, reduce the load carrying performance of a masonry wall. Research in the area of the masonry constructions made up of dry joints is therefore essential to understand their behaviour under compression. The following research will analyse the impact of height imperfection of individual masonry blocks on the in plane load bearing capacity of dry-stacked masonry walls. Based on the outcomes of the experimental researches of [20], a finite element model has been developed for the investigation of the load percolation in a wall. The paper is organized in three sections: while the first section gives an overview of the finite element modelling theory, the second section analyses the performing of the FE code for the study of the masonry block, in order to evaluate the accuracy of the numerical approach compared to the actual behaviour observed during the former experimental tests. Finally, the third

section studies the influence of the height imperfection of the masonry blocks on the load percolation in a wall including an approach to take into account its effects.

2. Material law and approaches for modelling

2.1. Material model

As many former authors have already highlighted [2–4,7,10,21], the load bearing capacity and the deformation of a masonry block is strongly characterized by a complex nonlinear behaviour due to the occurrence of cracks either in the block, in the mortar layer, or both. For the developed finite element model, the material nonlinearity in the compressive stress field is considered for the masonry block in the tri-dimensional directions. The stiffness matrix of the material is updated upon occurrence of cracks. Indeed, the effects of micro cracking are taken into account by the modification of the stress–strain relationship by means of the shear transfer coefficient defined by William and Warnke [21]. A multi-linear elastic approach is used to model the nonlinear stress–strain curve of material in the software.

The stress–strain behaviour of concrete (Eq. (1)) is modelled according to the prescriptions of Eurocode 2 for the nonlinear structural analysis of a concrete structure.

$$\sigma_c = (f_{ck} + 8)(k - \eta^2)/1 + (k - 2)\eta \tag{1}$$

$$k = 1,05E_{cm}|\varepsilon_{c1}|/(f_{ck} + 8) \tag{2}$$

$$\eta = \varepsilon_c/\varepsilon_{c1} \tag{3}$$

σ_c: Compressive stress at time 't' of the loading; $f_{ctm} = 0,3 * f_{ck}^{2/3}$: Ultimate tensile strength at 28 days; f_{ck}: Ultimate compression strength; E_{cm}: Elastic modulus of concrete; ε_{c1}: Strain at the ultimate stress; ε_c: Strain at time 't' of the loading.

2.2. Failure criterion

The failure criterion adopted for the finite element analysis is the yield criterion defined by William and Warnke [21]. The William and Warnke criterion is one of the common criterions used to predict failure in concrete and other cohesive-frictional materials. The criterion is given in function of three invariants, I_1, J_2 and J_3: the first invariant of the Cauchy stress tensor, the second and third invariants of the deviator part of the Cauchy stress tensor. In addition, the yield criterion takes as input five material parameters: the uniaxial compressive strength f_c, the uniaxial tensile strength f_t, the biaxial compressive strength f_{cp} and the shear transfer coefficients β_c and β_t. The failure criterion under multi-axial state of stress is given as it follows [6]:

$$\frac{F}{f_c} - S \geqslant 0 \tag{4}$$

F: Combination of principal stresses $(\sigma_1, \sigma_2, \sigma_3)$ in function of the state of stress; f_c: Ultimate stress strength in uniaxial compression; S: Failure surface expressed in function of the state of stress.

The combination of the principal stresses σ_1, σ_2 and σ_3 provides four different state of stress. For each state of stress, the failure surface S and the function F of the failure criterion are defined. The details of the calculation of the failure surface according to William and Warnke theory are given in [21].

The occurrence of any crack in the model is translated by the weakening of the stiffness matrix leading to a modification of the stress-strain relationship. According to William and Warnke, a weakness plane is defined in the normal direction to the crack surface and the shear strength of the cracked section is reduced by means of a shear transfer coefficient β_t and β_c for open and closed cracks. The nonlinear curve of the stress-strain response of the model is approached by a multi-linear stress-strain relationship where each linear step uses the generalized Hooke Law. Thus, for $\{\sigma\} = [D_i]\{\varepsilon\}$ describing the nonlinear stress-strain relationship, [Di] represents the stiffness matrix of the structure for load step i, $\{\sigma\} = [\sigma_x, \sigma_y, \sigma_z, \sigma_{xy}, \sigma_{yz}, \sigma_{xz}]^T$ and $\{\varepsilon\} = [\varepsilon_x, \varepsilon_y, \varepsilon_z, \varepsilon_{xy}, \varepsilon_{yz}, \varepsilon_{xz}]^T$ represent the stress and strain matrix. Following each crack, the initial stiffness matrix is updated by means of a shear transfer coefficient (β_t, β_c) and a secant modulus (R^t).

As already explained, the shear transfer coefficient (β) represents the conditions of transfer of the shear stress at the interface of cracking. The value of β_c and β_t varies between 0 and 1, with 1 representing a complete loss of shear transfer while 0 representing a rough crack with a good shear transfer. Uday et al. [8] have highlighted the fact that the ratio β_t/β_c and vice versa do not have much influence on the masonry strength.

2.3. Dry-joint model

The main difference between dry-stacked masonry and grouted masonry consists in the contact quality between two superimposed blocks. As aforesaid, the dry-stacking system leads to two major geometric imperfections: the local roughness of the contact areas (Δh) and the global height variation of the masonry block (ΔH). This paper studies solely the effect of the height imperfection ΔH whereas the roughness Δh is not taken into account. The dry joint was modelled using a regular disposition of LINK elements, which ensure a load transfer through the actual contact areas.

The LINK element is constituted by two nodes, connected by a line of an infinitesimal stiff cross-section and a Young modulus set 10 times higher than the one of the concrete used for the masonry block. The value of the Young modulus is fixed high enough to avoid any kind of longitudinal deformation. In addition, the LINK element is designed to work only in compression and not in tension, in order to allow a possible lifting of the masonry block in a wall under tensile stresses. Fig. 1 shows the stress–strain curve defined for the LINK elements.

3. Finite element modelling and results

3.1. Finite element modelling of the masonry block

A 3D micro-model with cracking and crushing capability has been implemented to simulate the behaviour of a dry-stacked masonry block (Fig. 2) under axial compression. The 3D micro-model allows a more accurate and general simulation of the masonry compressive strength due to the more realistic prediction of cracks patterns and their development. The accuracy of the

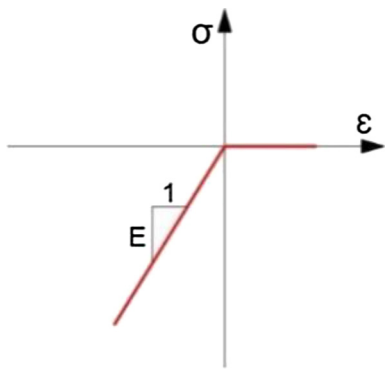

Fig. 1. Stress-strain relationship of the used LINK element.

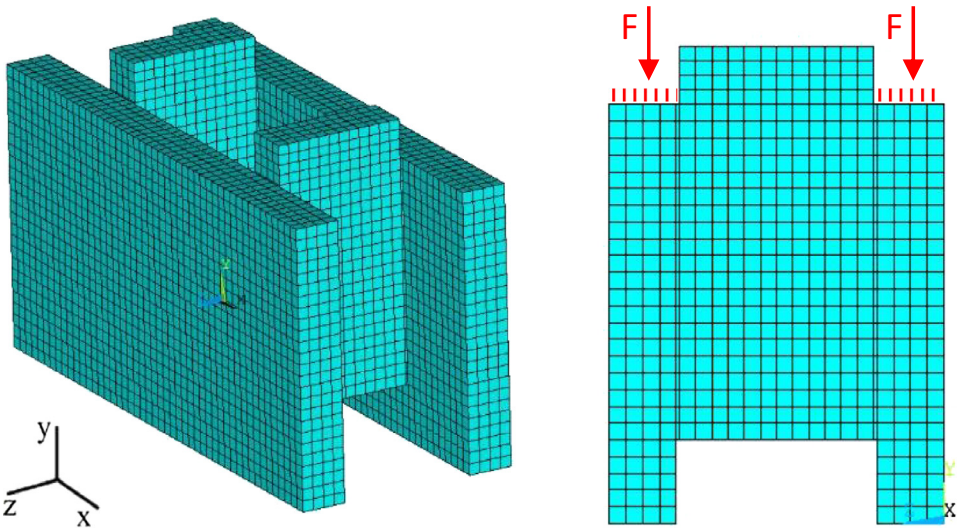

Fig. 2. Full 3D meshing of a masonry block with cubic elements of 10 × 10 × 10 mm.

model was checked by a comparison of the numerical outcomes with the experimental data. The studied masonry block is constituted by two face shells of 40 mm width, linked by two webs faces of 30 mm width. The block is modelled and meshed with cubic elements "SOLID65" provided by ANSYS17. This last element provides cracks and crushing capability and has a cubic shape with three degrees of freedom (translation x, y and z). Fig. 2 shows details of the full 3D regular mesh of the masonry used in the finite element model. The material properties of concrete are set as in the former experimental tests (Table 1), while the coefficients (β_t and β_c) of the shear transfer within cracks are calibrated and validated by outcomes of Uday [8]. The combination of $\beta_t = 0,2$ for the shear transfer in open crack and $\beta_c = 0,5$ for the shear transfer in closed cracked leaded to similar results as obtained in the experimental tests. The statement of Uday who highlighted the fact that the ratio β_t/β_c and vice versa do not have much influence on the masonry compressive strength could be confirmed.

For a clear discussion of the internal distribution of stresses, a coordinate system x–y–z was defined, with the x-axis parallel to the face shells, the y-axis normal to the loading plane of the masonry block and the z-axis normal to the face shell or parallel to the web face. In addition, in the experimental tests as in the finite element model, the masonry blocks are loaded solely along their face shells.

For the numerical analysis of the masonry block, the maximum estimated load was applied in thousand increments on the top areas of the face shell and a nonlinear analysis was carried out until convergence of the solution. Respecting the real boundary conditions of the experimental tests, the displacements in the three directions (ux, uy and uz) were restrained at the base of the block. According to Atkinson and Kingsley [24], the increase of failure stress due to edge effects is about 15% for concrete blocks.

Table 1
Material properties of concrete.

Concrete properties	
Ultimate compressive stress [MPa]	75
Ultimate traction stress [MPa]	7
Young's modulus [N/mm^2]	41,500
Poisson's ratio	0,2
Shear transfer coefficient for open crack, β_t	0,2
Shear transfer coefficient for closed crack, β_c	0,5

- At y = 0 mm, ux = uy = uz = 0
- At the top of the structure (masonry block or wall), ux = uz = 0

3.2. Finite element analysis and results

3.2.1. Load bearing behaviour of a single masonry block

Fig. 3 shows the stress distribution in the masonry block at 40% of the ultimate load (Fu). It is worth to remind that the specimen was loaded along the face shells as previously highlighted in Fig. 2. In the face shells, the compressive load is almost uniformly distributed. Nevertheless, a part of the compressive load is transmitted to the web faces concavely. In the web faces, the concave distribution of the compressive stress creates a tensile stress in the sections next to the lower and upper edges of the web, which can lead to failure when the tensile strength of the material is reached (Fig. 3). Fig. 4 shows the variation of the tensile stress in the web and the compression stress in the face shells, in function of the applied load. The compressive stress is measured at the middle height of the face shells, while the tensile stress is measured in the lower section of the web face as shown in Fig. 4. It can be observed that, in function of the loading, the compressive stress increases linearly in the face shell, whereas the tensile stress in the web face evolves non-linearly. One notes that until 50% of the ultimate load (Fu), the tensile stress evolves quickly in the web face and then, tends to stabilize beyond this load level. Indeed, the occurrence of cracks at the interface between the web face and the face shells (Fig. 5) is followed by a stress relaxation and a stabilization of the tensile stress in the web faces. At the same load level, the face shells are under compression with still a huge capacity to withstand compression. The failure of the masonry block occurs when the web faces fully crack, despite that the compression stress in the face shells remains far from its ultimate limit. This behaviour fits with that observed by some former authors such as Waleed [4], Agaajani [20], Jaafar [22] and Bronius [23].

In order to validate the developed FE model (load and behaviour prediction of the block), experimental tests were conducted on single masonry blocks exclusively loaded on their face shells as shown in Fig. 6. In order to ensure the exclusive application of the loading along the face shells of the blocks, stiff steel plates were added between the face shells of the masonry block and the press plate. At the failure of the masonry block, the experimental tests provided a maximum load Fu of 2080 kN as average, while the finite

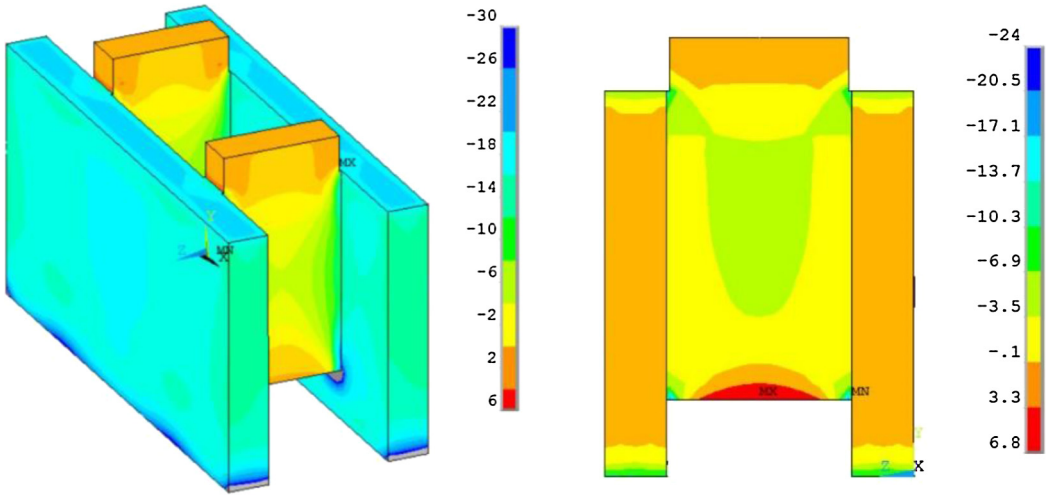

Fig. 3. Stress (σ_y) distribution at 40% of the ultimate load in a masonry block loaded on its face shells. Stress in y-direction [in MPa] (left side) and stress in z-direction [in MPa] (right side).

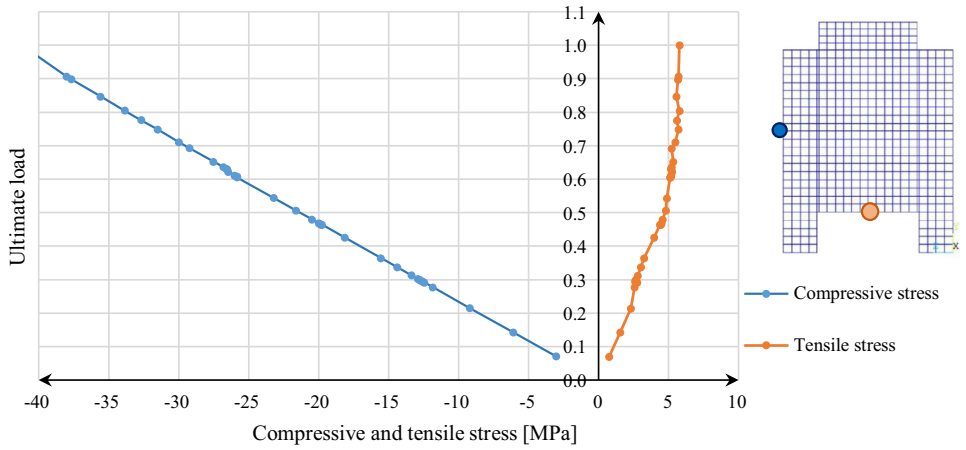

Fig. 4. Compressive stress σ_y in the face shell and tensile stress σ_z in the web face in function of the ultimate load.

element micro-model predicts a maximum loading of 2031 kN. Thereby, with the finite element model, the prediction of the load bearing capacity of the masonry block is possible with an accuracy of 97%.

Fig. 7 shows the cracking observed during the experimental campaign. This can be compared to Fig. 5 which shows the path and the evolution of the cracking predicted by the FE model. The experimental tests show that the single masonry block fails by appearance and development of cracks at the interface between the web face and the face shell. The same could also be observed in the results of the numerical model. In addition the FE prediction allows to show that the observed cracks appear firstly close to the upper and lower edges of the web faces at the interface between the face shells and the web faces. This effect is due to the concave distribution of the compressive stress in the web faces, which creates high tensile stress along this interface. The increase of the applied load leads to further tensile stress and cracking along the height of the web face. As the face shells detach from the web face, the lateral displacements of the face shells increases and thus, amplifies the cracks growth. In the present experimental investigation (Fig. 7), first noticeable cracks were observed in the masonry block at a loading of 10% of Fu, along the junction between the face shells and the web face. The FE model predicts the first cracks at the same location at a loading of 8% of the Fu. Indeed, it should be stressed out that probably during the experimental test, the first cracks appeared a little earlier but were not sufficiently visible to be already registered. Compared with the experimental outcomes, the finite element results show for the prediction of the crack path, as well as for the minimum cracking load, with an accuracy of around 80%, a good correlation with the experimental results.

3.2.2. Load bearing capacity of the masonry walls

Following the study of an isolated masonry block, masonry walls of various heights have been studied. The results of the experimental tests undertook on masonry walls and reported in [20] are used to validate the numerical model under in plane loading. The 3D micro-model developed for a single masonry block was extended to a wall, the interest of the 3D model being the visualization of the cracks occurring in the web faces in function of loading. The height to thickness ratio (h/e) of the tested walls was varied from 3,75 to 2,50 and the length was kept to 1 m. It has been reported in [20] that the support faces of all the masonry blocks used to build the wall were grinded to reduce the roughness of the contact surfaces and to reduce as well as far as possible the height differences between the single of masonry blocks. The walls were subjected to an axial compressive stress applied along the face shells of the blocks on the top course until failure in the experimental test as well as in the FE model. In the FE-model the

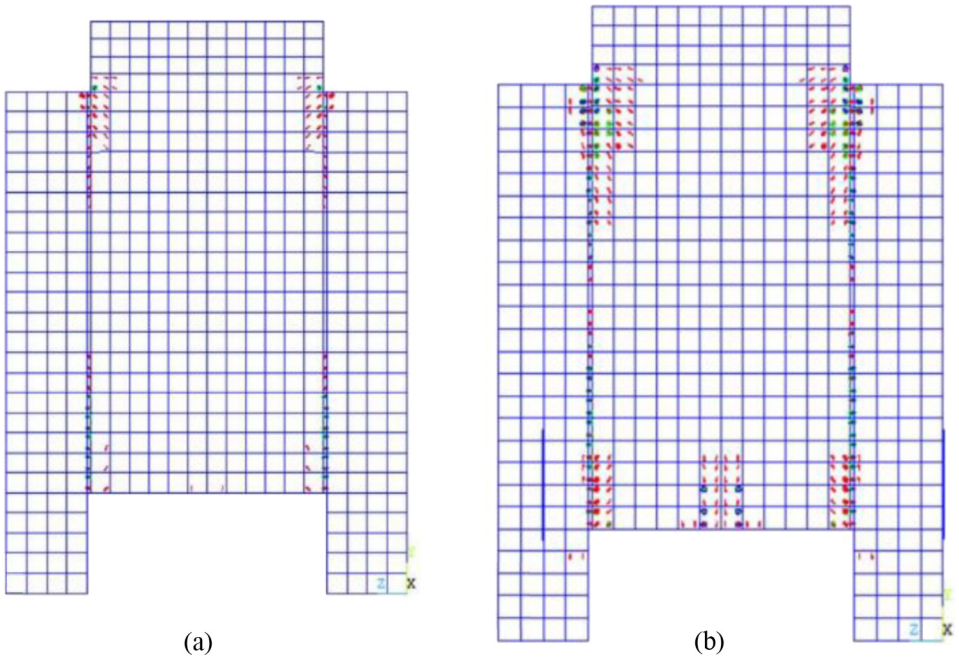

Fig. 5. Crack path prediction of the FE model at 10% of ultimate load (a) and at 80% of ultimate load (b).

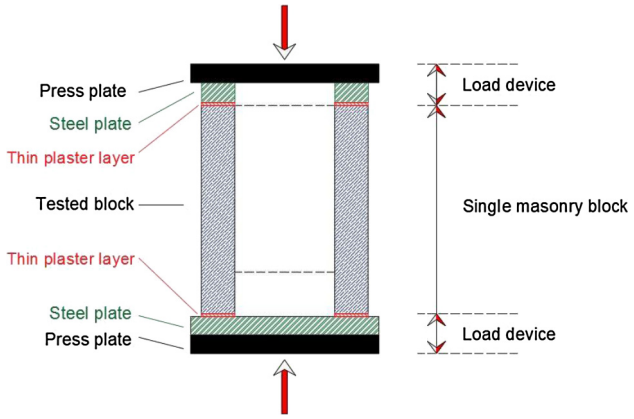

Fig. 6. Scheme of the experimental test on a single block.

cracking evolution could be analysed in detail. The two failure modes observed were a combination of face shell cracks and web face cracks. The cracking of the face shells appeared due to the existence of a height variation between the single masonry blocks.

In the present study, five walls with different h/e ratio were modelled, according to these former experimental investigations [20]. For the numerical model of the wall, the same material properties have been used as for the single block model (Table 1).

The investigation being focussed on the reduction of the in plane axial compressive load bearing capacity of a dry-stacked wall in function of the height variation of the masonry blocks, an x-y symmetry plane has been defined in the middle section of the masonry block. The symmetry plane, which is justified by the symmetry behaviour of the blocks in the x-y plane, enables to reduce the computational effort. Fig. 8 shows the variation of the gross bearing capacity of the walls (GBC_w) in function of the height to thickness ratio (h/e). The results of the FE model and the one of the laboratory test picked from literature [20] are plotted here. In the FE model as well as in the experimental investigation, the masonry blocks were only loaded on the top course of the walls along the face shells.

The gross bearing capacity of a wall (GBC_w) is obtained by dividing the ultimate load by the whole cross section of the wall (length × width). Table 2 summarizes the datasets and a comparison of the gross bearing capacity of walls obtained by experimental tests and by FE analysis. The relationship between the GBC_w and the ratio (h/e) is approached by a nonlinear curve more or less close to the experimental one. Indeed, unlike the close agreement found on a single masonry block, the finite element model slightly overestimates the gross bearing capacity of walls compared to the laboratory tests data [20]. It can be observed that the difference **ΔP** between the FE results and the experimental results increases with the increase of the ratio h/e. Indeed, these variations come from the geometric imperfections of the masonry blocks. The height variation of the masonry blocks used to construct the walls in the laboratory tests reduces the useful section theoretically available and prevents a uniform distribution and percolation of the load from one course to the underlying, thereby leading to a partial load concentration and a premature cracking of some masonry blocks. The numerical procedure shows very good agreements in the prediction of the capacity of the walls for a ratio h/e less than 6. For the ratio h/e greater than 6, the overestimation is about 15–20%, which is still interesting when referring to outcomes of Salah [16] and Anastasia [9]. It should be notified that the small gap of accuracy is due to the multiplication of imperfections in the walls with increasing h/e ratio. This may explain the slight overestimation of the bearing capacity provided by the numerical calculation as the height of the wall increases. Indeed, as the height of the wall increases, the geometric imperfections are summed up, thereby leading to a drop of the useful section of the walls. In return, the reduction of the useful section makes decrease the resistance of the wall (compared to the potential resistance that can provide a same wall without imperfections) Table 3.

4. Effect of the height imperfection on the stress distribution

During his experimental tests, Agaajani [20] has observed that due to the manufacturing process, in a sample of masonry blocks, the height distribution followed a Gaussian law. Based on its tolerance of production (±2 mm), a panel of different walls with masonry blocks of random height was modelled, Fig. 9 shows an

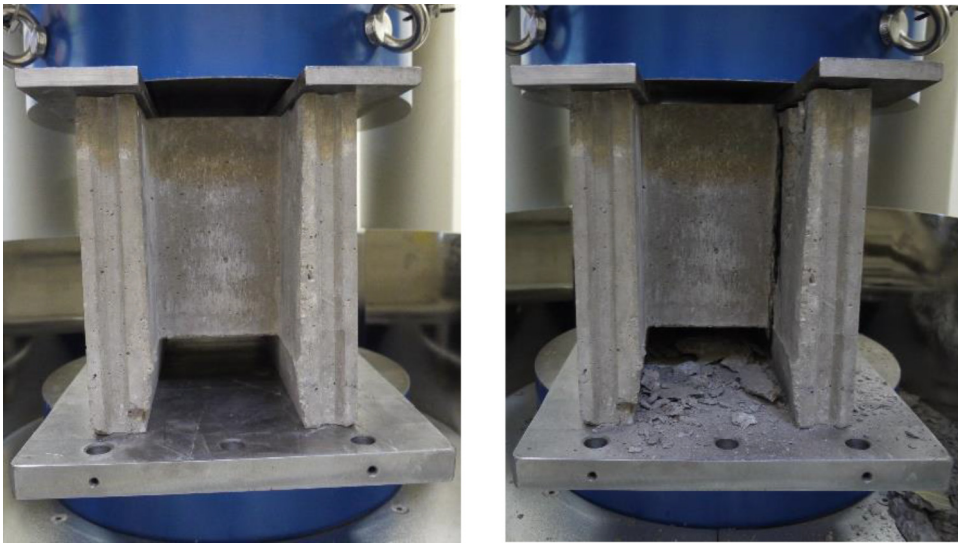

Fig. 7. Isolated masonry block before loading (a) and after failure (b).

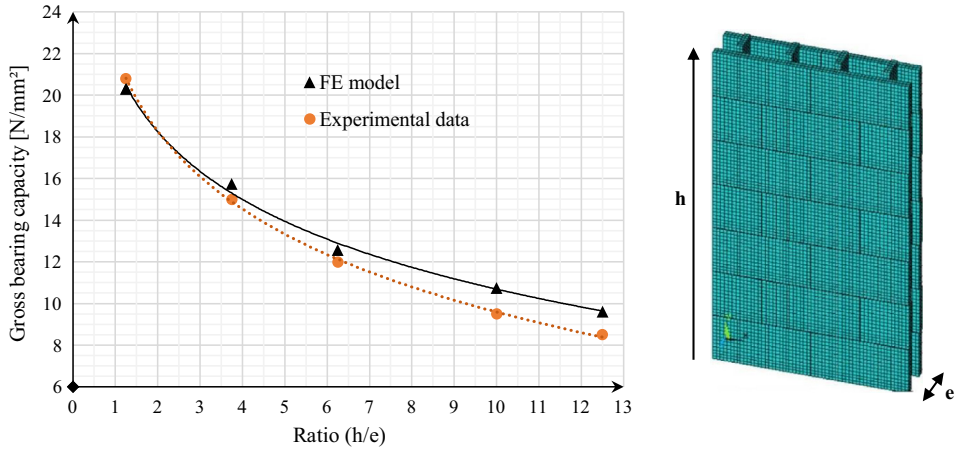

Fig. 8. Gross bearing capacity of the masonry wall in function of the height on thickness ratio h/e of the wall.

Table 2
Comparison of the gross bearing capacity of the wall from the FE analysis and from the laboratory tests.

Height [m]	h/e	$Experimental_{GBCw}$ [N/mm²]	FEM_{GBCw} [N/mm²]	ΔP
0,25	1,25	20,8	20,3	−3%
0,75	3,75	15,0	15,7	+5%
1,25	6,25	12,0	12,8	+7%
2,00	10,00	9,5	10,8	+14%
2,50	12,50	8,5	9,9	+17%

Table 3
Ultimate load of the masonry block in function of the load case.

Masonry load case	Ultimate load [kN]	Load reduction compared to load case 1 [%]
Case 1	2031	100,0
Case 2	804	39,6
Case 3	270	13,3
Case 4	810	39,9
Case 5	506	24,9

example. The analysis of the wall samples have allowed the definition of five load cases for a masonry block in a dry-stacked wall. Hereby, only the vertical load percolation trough the wall is considered. Indeed, the height variation of the masonry blocks from one course to the underlying one defines how each block will be loaded and supported. Fig. 9 shows the different possible worst-case scenarios for the vertical load percolation through individual masonry blocks.

4.1. Description and analysis of the main load cases of the dry-stacked masonry block

In the following step, the stress distribution on the actual contact areas will be defined as a function of the load case of the masonry block. For this purpose, a constant load of 100 kN is applied on the available loading areas of each masonry block.

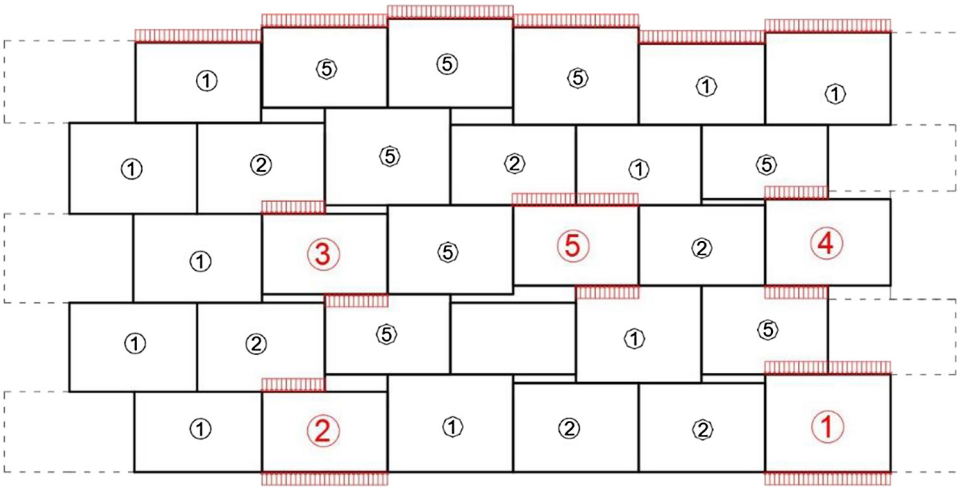

Fig. 9. Load cases (1–5) induced by the random height variation of the masonry blocks in a wall.

The stress distribution at the base of the masonry block is represented in Fig. 10 for each load case.

In the first load case, the masonry block is loaded and supported on its whole contact areas. For this case the applied load follows a vertical path, resulting in a uniform distribution of stresses at the contact area of the masonry as shown in Fig. 10. In this perfect case, the masonry block develops its whole resistance and cracks appear only along the height of the two web faces as already explained inSection 3.2.1. The lateral displacement along the upper face of the face shell is almost uniform in the whole masonry block. This load case occurs if all the masonry blocks of the wall have exactly the same height, or if there is a mortar layer between the different courses of the masonry blocks to ensure the levelling of the height differences.

Instead of a perfect vertical load percolation as observed in the first load case, the numerical analysis of the load cases 2–5 shows a specific non-uniform load distribution. For the second load case, the masonry block is loaded on one-half section and supported on its whole contact area. As highlighted in Fig. 10, 34% of the cross section carries 62% of the applied load whereas 16% of the cross section carries 18% of the applied load. The remaining load passes through the second half part of the cross section. Because of the non-uniform state of stress in the two half parts of the face shell of the masonry block, a shear stress is developed over the height of the face shell and it leads to premature cracking. Also, due to the non-uniform stress state in the two half parts of the face shell, a lateral displacement (z-axis) of the web face happens only on the loaded side of the block. The non-uniform lateral displacement of the whole masonry block leads to the development of cracks in the web face (along the interface with the face shell) of the loaded side. The ultimate load of the masonry block is thus reduced by 60%. Here the applied load follows a vertical path in the loaded side and an oblique path in the unloaded side (right side).

In the third load case, the masonry block is loaded on one-half cross section and supported on the opposite half cross section. This support configuration comes from the gap between the different masonry blocks of the analysed course and of the underlying course. Here, due to the asymmetrical disposition of the loaded area with respect to the support area, one might think that the masonry block is likely to spin instantly upon loading. In fact, although occurring, this movement is more or less limited or prevented by the neighbouring blocks of the considered course (Fig. 11a and b). Depending on whether the underlying gap to cover will be large, the masonry block will not move. Nevertheless, as the considered block will gradually deform and remains supported on two small sections (the middle section and one of the left or right end section), a load redistribution will occur. Considering the afore-mentioned load and support conditions, the block was modelled in a way to respect the real boundary conditions by limiting the displacement along the x-axis by neighbouring blocks. On the left and right sides of the masonry block, contact and spring elements were arranged to simulate the resistance to horizontal displacement imposed to any neighbouring blocks of the considered course (Fig. 11b). The spring elements were designed to provide a very low compressive strength and a null tensile strength (Fig. 1), thus leaving each masonry block the flexibility to displace. Upon loading, a slight spin of the masonry block occurs and a great part of the applied load is carried by a small part of the lower cross section. As it can be observed in Fig. 10 (load case 3), a uniform load applied on top of the masonry block produces a stress concentration at the lower contact face. Moreover, it is observed that 60% of the applied load is transferred through solely 18% of the cross section of the masonry block. The remaining 40% of the applied load is transmitted across 32% of the cross section. The stresses concentration is heightened in the middle of the cross section, which results in a swift increase of the shear intensity in the critical section and a swift growth of cracks. Nevertheless, the continuous deformation of the masonry block allows at a certain moment to increase the actual contact surface of the block, which then enables a load sharing in the wall. This load case is the most unfavourable compared to the four other. The compressive strength of the masonry bock is reduced by 86% and the applied load follows an oblique path of at most 63° ($\alpha = \tan^{-1}$[length/ height]).

In the fourth load case, the masonry block is loaded and supported on a whole side, along a half cross section of the masonry block. Here, the full masonry block behaves like two distinct half blocks, the first being uniformly loaded and supported on its whole contact area, the second being not loaded. As highlighted in Fig. 10 (load case 4), the applied load is uniformly distributed on one-half cross section. In this load case, premature cracking appears in the middle of the masonry block, as a straight line along the height of the face shell. The out of plane displacement of the upper side of the face shell is irregular along the masonry block. The out-of-plane displacements occurring on the loaded side of the block intensifies the cracking of the web face of this side. These phenomena reduce the compressive strength of the masonry block by 60%.

The last load case is the one where the masonry block is loaded on its whole cross section and supported on a half cross section. In this load case as in the third load case, one might think that the block will simply spin, but the flexibility of a masonry block to spin

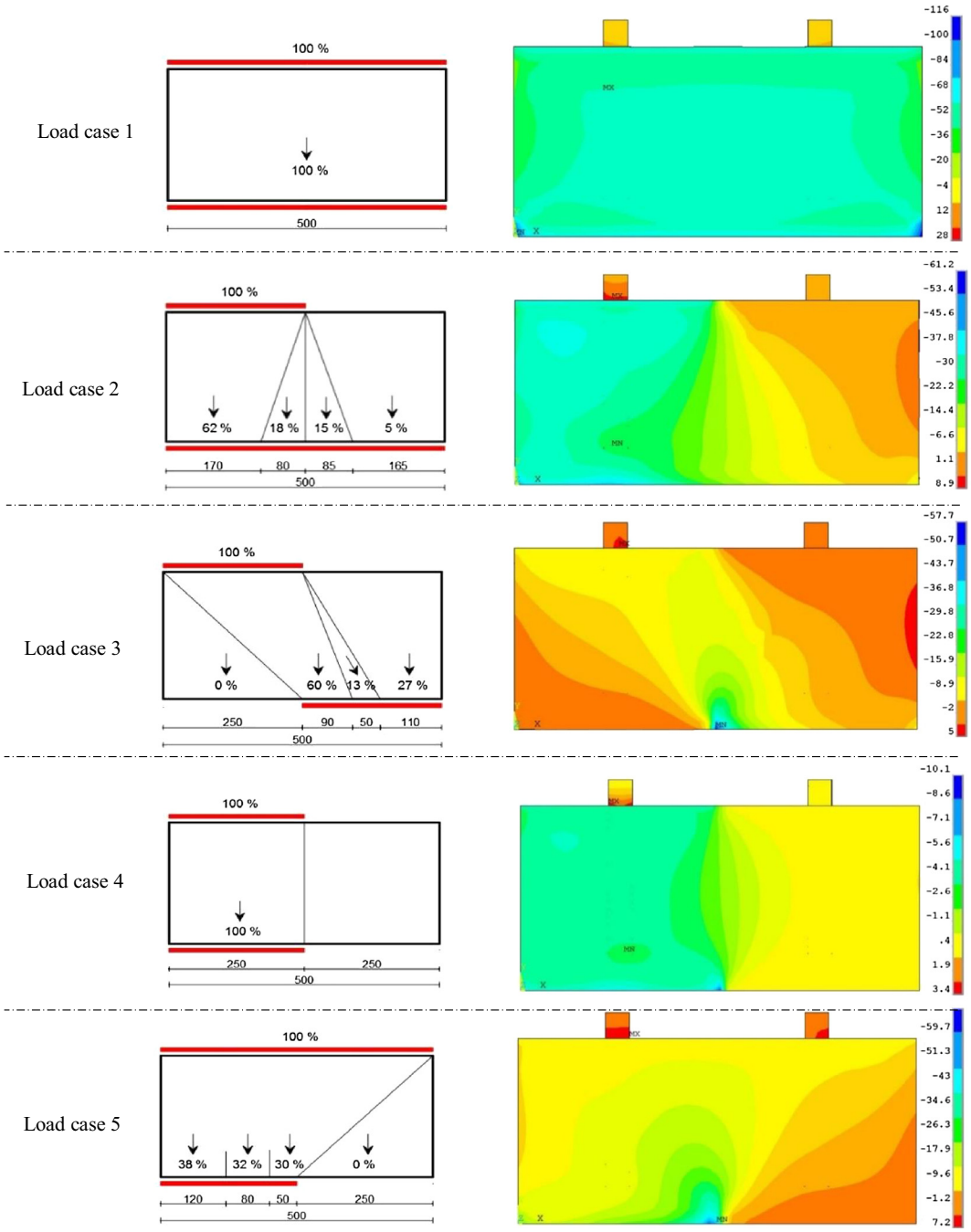

Fig. 10. Stress distribution [MPa] in the masonry block in function of the load case. (length of the block = 500 mm).

is depending on the position of the masonry block in the wall, whether it is in the upper course or elsewhere. Indeed, as shown on Fig. 11, a spin of any masonry block requires vertical and horizontal displacement of the block. However, each masonry block is not fully free to move along the x-axis due to its neighbouring blocks (Fig. 11b). In addition, in all the courses other than the upper course of the wall, the masonry block is only able to spin if on one side at least the weight of all the overlying courses can be lifted. Theses combined effects of the weight and the interaction between the blocks in a course limits the movability of the blocks in a wall. Nevertheless, as in the previous cases, the increase of the in plane displacement will finally lead to an increase of the contact surface between the courses. This load case produces a load concentration at the middle of the masonry block. As it is shown on Fig. 10 (load case 5), 30% of the applied load passes through 10% of the cross section and the remaining load is distributed on 40% of the cross section. Due to the load concentration in the middle of the masonry block, high shear stresses are developed, which gives rise to cracking. As for load case 2, the stresses follow a vertical path above the supported side and an oblique path of at most 63° in the unloaded side of the masonry block. The premature occurrence of cracks is responsible of a reduction of 75% of the compressive strength of the masonry block.

Fig. 11 shows a reduced model of a wall with the contact and spring elements provided to model the vertical and horizontal interaction between the masonry blocks. Fig. 11a shows an initial positioning of the masonry blocks before loading, while Fig. 11b shows the vertical and horizontal interactions with rotation occur-

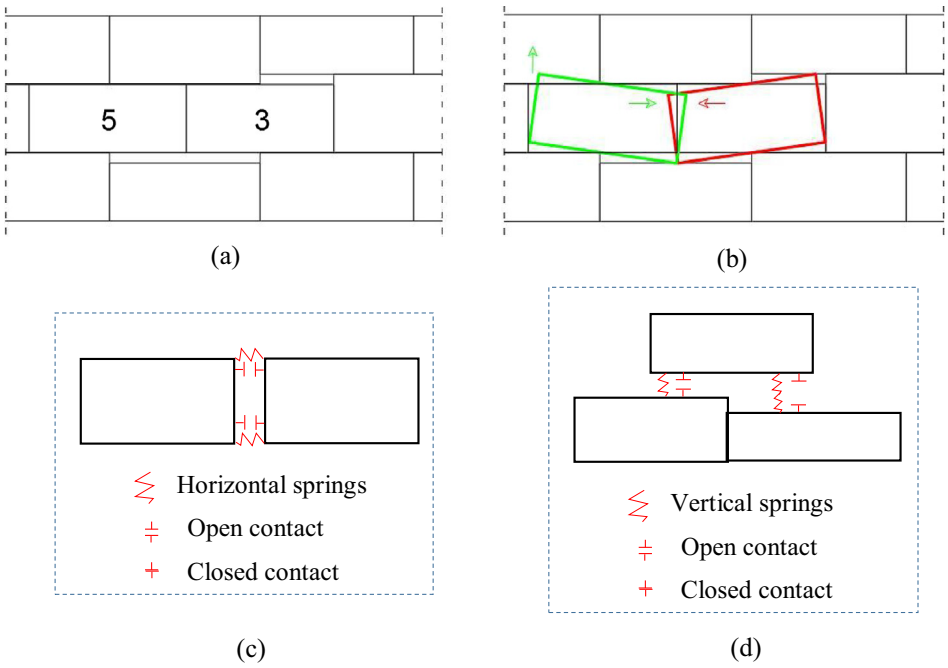

Fig. 11. Loading and boundary conditions schemes for the load cases 3 and 5. (a) Initial positioning of the masonry blocks; (b) interaction occurring between the masonry blocks under loading; (c, d) contact and spring elements on the edge faces of the masonry blocks.

ring between the two blocks that may spin if it would the blocks would be free to rotate. The spring and contact elements defined on the vertical and horizontal edge faces of the masonry blocks (Fig. 11a and b) enable to ensure the vertical load transmission as well as the horizontal interaction between the blocks in the load cases 3 and 5. In these load cases the horizontal interaction (Fig. 11b) limits already the rotation of the masonry blocks which is still reinforced by the fact that the block needs to overcome first the vertical loading including self-weight of the overlying courses before a rotation can take place.

4.2. Effect of the height imperfection ΔH of the masonry blocks on the load percolation in a wall

A finite element analysis was performed on a set of walls built with masonry blocks of random height and selected within the statistical height distribution measured on manufactured blocks [20]. Table 1 sets the material properties used to model the walls and the latter walls are gradually loaded on its top areas. Given that the computation time of a large-scale wall is very important, an x-y plane of symmetry was defined and the size of the studied walls limited to 3 blocks in the length and 5 in the height. Fig. 12 shows two load percolation systems which can occur in such a wall. These latter systems are used as an example for perceiving the unpredictable effect of the geometric imperfections of the masonry block on the load bearing capacity of a wall. In Fig. 12, Δ represents the height imperfection of each masonry block with respect to the theoretical height in millimetre.

Due to imperfections, the first wall reached failure at 260 kN, thus at 24% of the ultimate load of a same wall without imperfections (ultimate load, 1100 kN). Concerning the second wall, the failure appeared earlier at 60 kN, thus at only 5,4% of the ultimate load of a same wall without imperfections. Fig. 12 also highlights the load percolation in each wall, while showing the different load cases of the masonry blocks as described in the previous section. Based on the load cases of the masonry blocks appearing in each wall, one can describe why wall B reached failure earlier than wall A.

Wall A is progressively loaded on the top course (R5 in Fig. 12a) with increments of 10 kN till the ultimate load of 260 kN, which corresponds to a stress of barely 1,5 N/mm^2. The three masonry blocks of course R5 are uniformly loaded and their load cases are similar to load case 5. This being, premature cracking occurs and according to the previous findings, the failure of these masonry blocks is predicted at 24% of the ultimate load of an isolated masonry block. The applied load percolates in contact area C4, through one and a half block. Instead of a cross section of 1000 × 175 mm^2, the load passes through an actual section of 525 × 175 mm^2, which corresponds to a local stress of 2,82 N/mm^2. Due to the height imperfection of the masonry blocks, the actual contact area C4 is reduced and the stress is almost doubled in course R4. This phenomenon explains the increase of stress intensity observed in the masonry blocks of course R4 where only two blocks participate to the load percolation. The load case of the first masonry block corresponds to load case 5, while the load case of the second masonry block corresponds to load case 4. One more time, because of the height imperfection of the masonry in the underlying course R3, the actual contact at the contact area C3 is reduced to a cross-section of 350 × 175 mm^2 (two half blocks). The drop of the cross section implies an increase of the stress from 2,82 N/mm^2 to 4,24 N/mm^2 in course R3. Between the three masonry blocks of course R3, only two participate to the load percolation. The first masonry block is loaded according to load case 4 and the second masonry block according to load case 3, which is the most critical one. In this course (R3), the cracking of the face shells of the two bearing masonry blocks is predicted to 12% of the ultimate load of an isolated masonry block. Here the stress in the top face of the masonry block is no longer evenly distributed, thus leading to much more load concentration and early cracks. In the contact area C2, the available cross section for the load percolation is the same as in the contact area C3, thus the mean stress remains steady from course R3 to course R2. However, the local stress peak observed in the contact area C2 highlights the effect

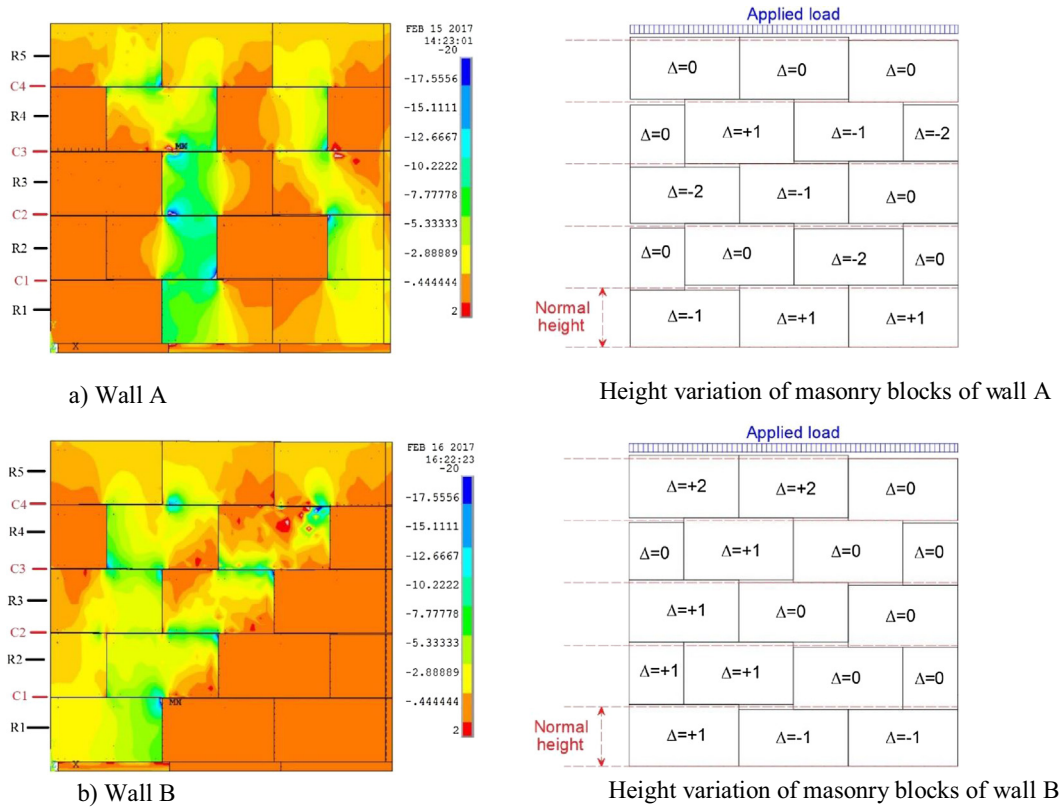

Fig. 12. a) Stress distribution σ_y [MPa] in wall A (ultimate load = 260 kN); b) Stress distribution σ_y [MPa] in wall B (ultimate load = 60 kN).

of the concentrated load coming from the above block. In fact, as afore mentioned, the first full block of course R4 is in load case 5, thereby it transfers a part of the load in a point load. The effect of the concentrated load appears on the left upper corner of the second masonry of course R3 as a local peak stress followed by cracking (Fig. 13). The same observation is established on the second branch of the load percolation system. The third masonry block of the fifth course partly transfers its load by a concentrated load applied on the right upper corner of the second full block of course R4. This point load is almost transferred from the upper corner to the lower corner and the cracking of the third masonry block of course R3 (Fig. 13) highlights the intensity of the point load. The transfer of the load through contact area C1 is carried out without special features, as the cross section remains the same from C2 to C1. Finally, in course R1, only two masonry blocks bear the whole applied load. Each of these blocks is similar to the masonry defined in load case 2: only 50% of the support area of each masonry block support 80% of the applied load. One observes that the stress intensity in the two masonry blocks of this last course is slightly lower than the one observed in course R2, merely because of the increase of the actual contact area on the bottom faces. Nevertheless, the stress intensity of these masonry blocs remains higher and far from the one of the masonry blocks in course R5. On Fig. 13, the appearance of cracks at low level of load (9% of the ultimate load) in the face shells of the masonry blocks point out the harmful effect of the height variation of the blocks. This premature development of cracks limits the serviceability load of dry-stacked walls.

Table 4 displays the results of Fig. 12 for blocks taken individually. It represents the contact stress, the actual contact area as well as the different load cases of the masonry blocks of course R1, R3

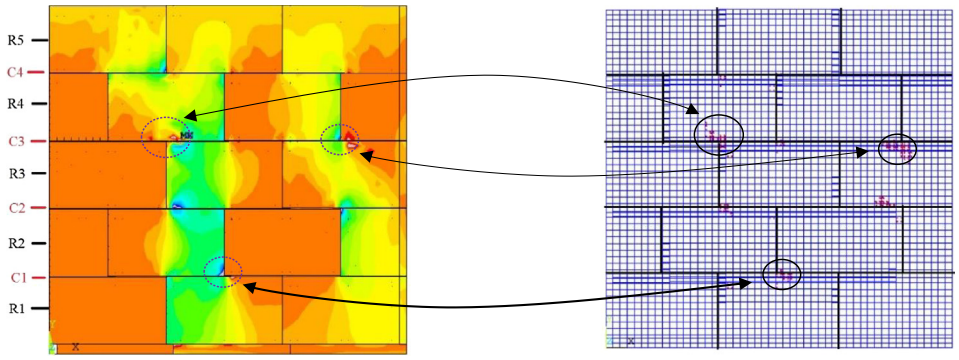

Fig. 13. Stress distribution and crack path in wall A at 9% of ultimate load.

Table 4
Loads cases and actual contact area in walls A and B for masonry course R1, R3 and R5.

Wall A

Course		Masonry block 1			Masonry bloc 2			Masonry bloc 3		
		Load case	Actual contact area [%]	Max. stress [MPa]	Load case	Actual contact area [%]	Max. stress [MPa]	Load case	Actual contact area [%]	Max. stress [MPa]
R5	Top	5	100%	1,48	5	100%	1,48	5	100%	1,48
	Bottom		50%	2,97		50%	2,97		50%	2,97
R3	Top	–	0%	0	4	50%	2,97	3	50%	2,97
	Bottom		0%	0		50%	5,94		50%	2,97
R1	Top	–	0%	0	2	50%	5,94	2	50%	2,97
	bottom		0%	0		100%	2,97		100%	1,48

Wall B

Course		Masonry block 1			Masonry block 2			Masonry block 3		
		Load case	Actual contact area (%)	Max. stress (MPa)	Load case	Actual contact area (%)	Max. stress (MPa)	Load case	Actual contact area (%)	Max. stress (MPa)
R5	Top	5	100%	1,48	5	100%	1,48	5	100%	1,48
	Bottom		50%	2,97		50%	2,97		50%	2,97
R3	Top	2	50%	5,94	3	50%	2,97	–	0%	0
	Bottom		100%	2,97		50%	2,97		0%	0
R1	Top	1	100%	4,45	–	0%		–	0%	0
	Bottom		100%	4,45		0%			0%	0

and R5 of the walls A and B. The analysis of the results of Fig. 12 grouped together in Table 4 enables to highlight some key findings:

- For a constant load applied on the top course of a wall, the geometric imperfections of the masonry blocks amplifies the stress intensity in the wall by a factor of proportionality which depends on the load percolation system;
- The applied load is more concentrated in the intermediate courses than in the upper course of the wall;
- The height imperfection of the masonry blocks in a course governs the load case of each masonry block, which therefore governs the load percolation system and finally the bearing capacity of the wall.

Due to the slight height variation of the different masonry blocks, the stress of 2,2 MPa evenly applied on the top course of wall A is unevenly distributed across the different contact layers from C4 to C1to the bottom face of the wall. For this model, at the base of the wall, the masonry block located between x = 0 and x = 350 mm does not participate at all to the load transfer of the wall. From 600 mm to 850 mm, the stress intensity is lower than the applied stress while in the remaining part of the wall, it is higher than the applied stress with an amplification factor up to 7. In Fig. 14, the curves C1 to C4 show the compression stress distribution over the length of the wall for each of the four contact layers; these specific curves illustrate how the load is unevenly transferred within the wall. On curves C2 and C4, one observes the stress peaks, which come from the concentrated loads, resulting themselves of the load and support conditions of the overlying blocks. In the wall B, most of the masonry blocks behave according to load case 3 as already explained in the previous section. The height variation of the masonry leads to a concentration of the load and the peak stresses reach almost 8 times the uniformly applied loading on the top course of the wall. Indeed, the abundance of stress peaks reflects the high concentration of loads on a small cross section of the masonry blocks at each contact layer. This last phenomenon is a result of the load and support conditions of the masonry blocks. Fig. 15 shows the progressive load percolation in the wall A.

In order to take into account the effect of the height imperfection ΔH, it is worth to define the useful section of a dry-stacked wall. In this purpose, to predict an optimal useful section, it is necessary to gather and study all the load percolation systems which

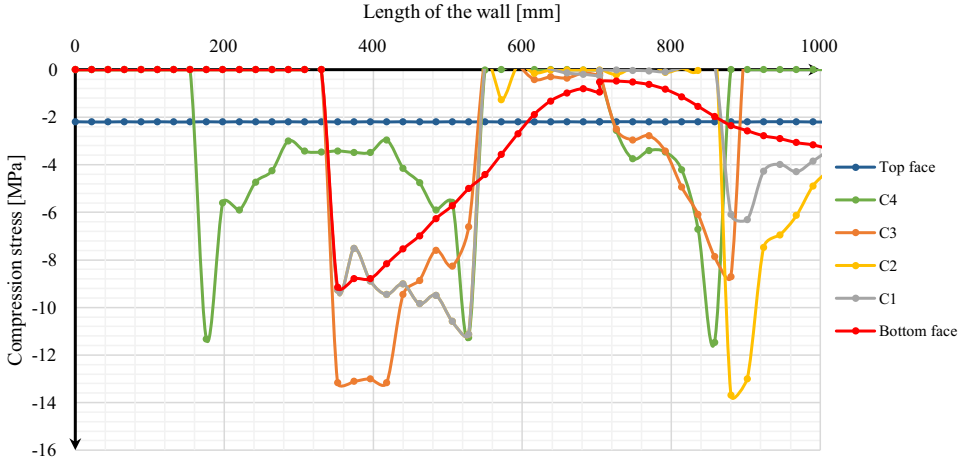

Fig. 14. Compression stresses at each contact layer and on top and bottom face of wall A.

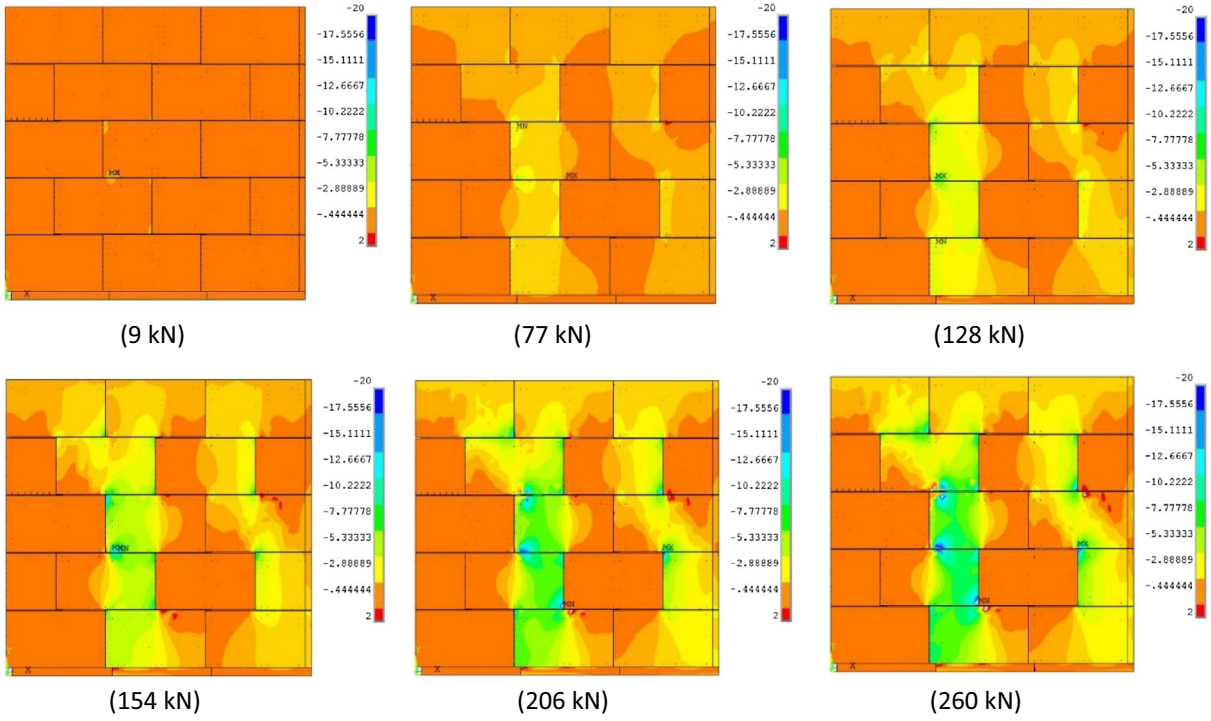

Fig. 15. σ_y stress [MPa] distribution over the height of the wall A, for the six different load steps.

can occur in a wall. From the latter systems, the most probable systems are deduced as well as their influence on the load bearing capacity of the wall. In addition, it should be noted that the appearance of cracks in the face shells of the masonry blocks is likely to change the load percolation system of a wall. In the following, the stress multiplier coefficient for respecting the reduction of the load bearing capacity due to the height imperfection ΔH will be evaluated for the uncracked state representing the most critical one.

4.3. Determination of the stress multiplier coefficient and the maximum compression stress of a masonry wall

The approach consists in defining an equivalent section coefficient k_{uE} calculated on the basis of all the possible load percolation systems in a wall of a given height and length. For a given wall with x masonry blocks in the length and y in the height, there is a large range of possible load percolation systems. From an analysis of the combinations of the load percolations systems, it has been observed that the number of load percolation systems (N) follows a logarithmic evolution with increase of the height and length of

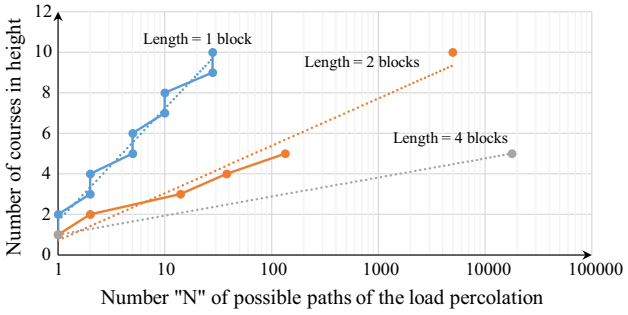

Fig. 16. Number of different load percolation systems depending on the height and length of a wall.

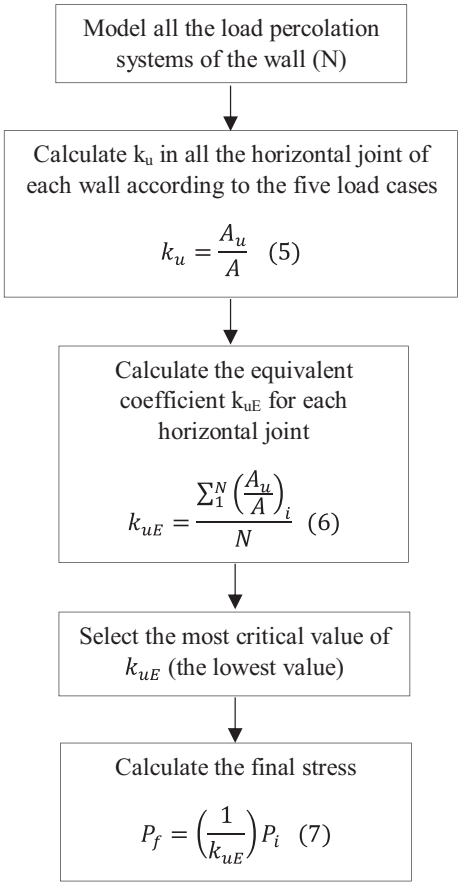

Fig. 17. Algorithm for the determination of the amplified stress due to the geometric imperfections of the masonry block.

the wall. Fig. 16 shows the number of load percolation systems in function of the height and the length of a wall.

In a wall, the different load cases of the masonry blocks enable to draw the load percolation system from which the rate of the actual contact or the useful contact (A_u) between the horizontal joins is deduced. Fig. 17 shows the flowchart of the algorithm for the determination of the equivalent useful section coefficient k_{uE}, leading to the maximum stress in the wall by taking into consideration the imperfections ΔH. The useful coefficient k_u in each horizontal join of each load percolation system is obtained by the ratio of the actual contact area (A_u) on the whole contact area (A), Eq. (5). Once the useful coefficient k_u calculated, the equivalent coefficient k_{uE} has been deduced by making for each join the average of the coefficient k_u, see Eq. (6). The relevance of the equivalent coefficient k_{uE} is related to the number of load percolation systems studied. If the number of percolation systems increase, the mean value of the useful section becomes more accurate. Following the calculation of the coefficient k_{uE} at each horizontal layer, the lowest value is selected to calculate the maximum stress multiplier coefficient (see Eq. (7)).

To show the interest of the method, a small wall built up of two blocks in the length and three blocks in the height has been studied. A constant stress of 9 N/mm^2 has been applied on the top of the wall.

First, all possible load percolation systems are determined by means of a finite element model (Fig. 18) and the compression stress is recorded at the base of the wall (Fig. 19). Based on the distribution plotted in Fig. 19, the stress intensity at each point of the lower contact area can be exactly indicated. Furthermore, the envelop curve (green curve) covering the effect of all the load percolation systems can be defined. Based on the shape of the envelope curve, it can be observed that the maximum stress intensity is strongly increased compared to the applied load. The multiplier factor of the stress goes up to 2,7 (9/25 [N/mm^2/N/mm^2]). This approach permits to predict the crack pattern and the actual behaviour of the wall, but it requires much computational time, and even more if the size of the wall increases.

The crack path and the load bearing capacity of the dry-stacked masonry wall are governed by the load cases of its masonry blocks, themselves governed by the imperfections ΔH. As an illustration, compared to the ideal wall number 1, the walls 2, 3, 4 and 5 reach failure respectively at 46%, 48%, 49% and 65% of the ultimate load of wall 1. In the same way, walls 6, 7, 8, 9 and 10 reach failure respectively at 34%, 65%, 39%, 39% and 33% of the ultimate load of the ideal wall. Indeed, the geometric imperfections, especially the height variation of the blocks, impose a path to the load percolation, which very often lead to a concentration of the load in some masonry blocks of the wall. Thus, the failure load of some masonry blocks is reached despite the fact that the load applied on the top of the wall is far from the ultimate load of the masonry block.

In the second approach, the flowchart defined in Fig. 17 to predict the maximum stress in the wall is applied. According to the findings of Fig. 17, it is known that a wall with two blocks in the length and three courses in the height counts up to 10 load percolation systems. For each of the ten load percolation systems, the useful coefficient k_u in each horizontal layer is calculated and the equivalent useful coefficient k_{uE} is deduced. Table 5 summarizes the obtained results. The critical value of the equivalent coefficient k_{uE} is for this approach 0,47and thus, the multiplier factor of the stress is therefore 1/0,47 = 2,1.

The numerical analysis enables to find a multiplier factor of 2,7 with a maximum compression stress of 25 N/mm^2, while, the analytical approach enables to find a multiplier factor of 2,1 with a maximum compression stress of 19,7 N/mm^2.

5. Conclusion

The lack of the mortar layer leaves place to geometric imperfections in the masonry walls due to two different kinds of imperfection of the masonry blocks: the height imperfection ΔH and the roughness of the contact areas Δh. The latter imperfections, especially Δh, are known to have high impacts on the load bearing capacity of the dry-stacked masonry wall. Many attempts have been undertaken to master the mechanical behaviour of dry-stacked masonry blocks and their outcomes have given a great boost to scientific advances. Among others, the developed empirical formula [6] and the homogenisation technique [10,11,15] developed to predict the compressive strength and the failure modes of dry stacked masonry blocks. Nonetheless, the impact of the geometric imperfections ΔH on the bearing capacity of dry-stacked masonry walls was still unexplained. Hence, the purpose of the paper is to describe the influence of the imperfections ΔH and proposes a way to calculate the load bearing capacity by considering them. Following many former authors, within this work a FEM was performed on a 3D masonry block to predict its mechanical behaviour and highlight the impacts of the geometric imperfection on the bearing capacity of a wall. The numerical model was performed using the William and Warnke criterion [21] and a multi-linear elastic stress–strain relationship was used to model the nonlinear behaviour of the masonry block on the ANSYS 17 software. Next to the numerical developments, an analytical approach based on the load percolation systems and the actual contact was developed to foresee the maximum compression

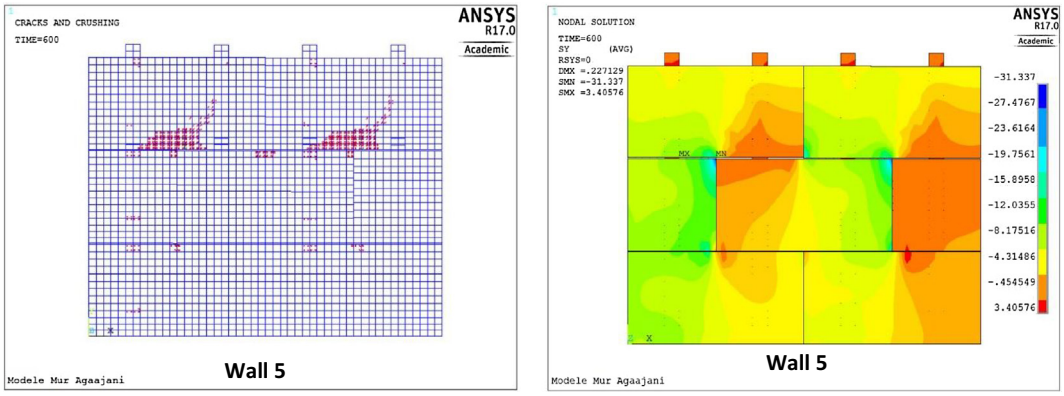

Fig. 18. Crack path and σy stress distribution [MPa] shown exemplarily by one load percolation system of a wall of 2 × 3 blocks.

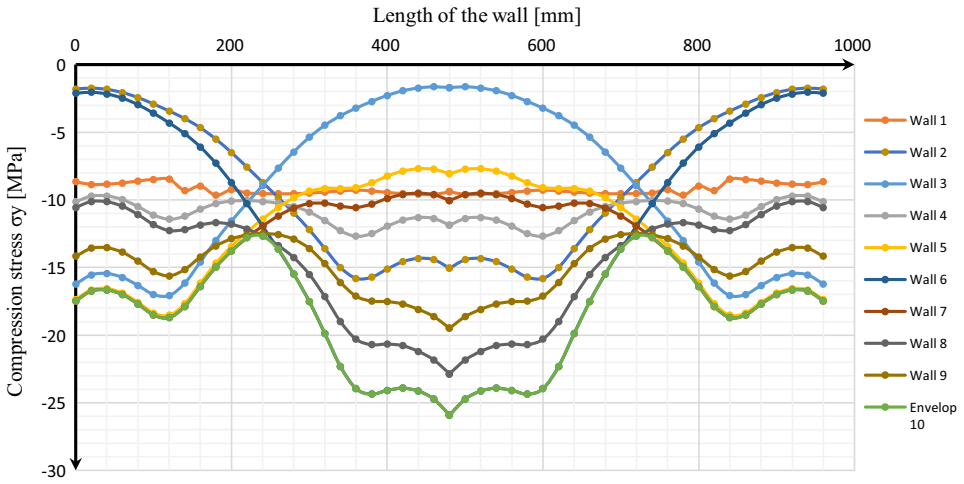

Fig. 19. Compression stress intensity recorded on the support area of the wall in function of different wall configurations and wall lengths.

Table 5
Calculation of the equivalent useful section of a wall of 2 blocks in the length and 3 in the height.

	k_u										k_{uE}	Critical k_{uE}
	Wall 1	Wall 2	Wall 3	Wall 4	Wall 5	Wall 6	Wall 7	Wall 8	Wall 9	Wall 10		
#3	1	1	1	1	1	1	1	1	1	1	1	0,47
#2	1	0,5	0,5	0,75	0,5	0,5	0,75	0,75	0,5	0,5	0,52	
#1	1	0,5	0,5	0,75	0,75	0,25	0,75	0,5	0,5	0,25	0,47	
#0	1	1	1	1	1	1	1	1	1	1	1	

stress deriving from the load amplification by the geometrical imperfections for an uncracked wall.

The next highlights summarize the main conclusions:

1. The developed 3D finite element micro-model enables to master the behaviour of the masonry block, predict its compressive strength and its failure mode with an accuracy slightly above 97% compared to the experimental results.
2. Although the hollow concrete masonry block is subjected to an axial compression, it shows a complex failure mode. As observed in the numerical models, the failure of the masonry block occurs following the development of cracks along the height of the shell and web face of the masonry block.
3. The height of each masonry block plays a crucial role in the response of a dry-staked wall under axial compression. Indeed, the height imperfection governs the rate of actual contact between the adjacent masonry courses, and thus, governs the load percolation system occurring in the wall.
4. In a dry-stacked masonry block, five load cases can be observed according to the height variation of blocks.

Load case 1:
The applied load is uniformly transmitted on the bearing faces of the masonry block. This load case represents the singular case of a traditional grouted masonry block where each masonry block is uniformly supported on its support areas. Here the masonry block behaves like traditional dry-stacked block and develops 100% of its bearing capacity.

Load case 2:
The masonry block is loaded on a half cross section and supported on its full cross section. However, the stress is unevenly distributed on the support face and up to 80% of the applied load passes through a half cross-section. The unevenness of the stress intensity in the face shell leads to shear and cracking, thereby restricting the masonry block to develop only 40% of its bearing capacity.

Load case 3:
Load case 3 is the most critical one. The masonry block is loaded on a half cross-section and supported on the opposite half cross-section; thereby 60% of the uniform applied load is transmitted on the lower contact area as a punctual load. The concentration of load precipitates the failure of the masonry block, which develops barely 13% of its bearing capacity. Nevertheless, although the simple spin of the masonry block is limited by the vertical and horizontal interaction between the adjacent blocks, it occurs progressively and leads to a wider load transmission in the underlying courses of a wall.

Load case 4:
In load case 4, the masonry block is loaded and supported on a half cross-section. The applied load follows a vertical path on the loaded side of the masonry block and only this part participates to the load percolation. The masonry block develops nearly 40% of its bearing capacity and the difference of the state of stress in the two parts of the face shell leads the vertical cracking in the middle of the masonry block.

Load case 5:
In the load case 5, the masonry block develops about 25% of its bearing capacity. Behind the load case 3, this load case is the second most unfavourable, because 30% of the uniform applied load is transmitted as an almost concentrated load. As in the load case 3, although limited, the progressive deformation of the masonry block may lead to a load sharing in the underlying courses.

5. The useful section of a dry-stacked masonry wall is function of the height and length of the wall. Indeed, more the height and length are increased more the useful section is statistically reduced.
6. The analytical approach for the determination of the maximum stress coefficient enables to find results close to the numerical ones. Compared to the numerical outcomes, it enables to predict around 80% (19,7/25 N/mm^2) of the maximum compression stress with less computational needs.

This paper enables to understand the effect of the geometric imperfection on the dry-stacked masonry blocks, but furthermore it proposes a new approach enabling to foresee the stress amplification in a wall, while taking into account the effect of the height imperfection ΔH. Thus, the findings of the paper could be used in various ways, either to assess the useful section of a wall, either to assess the stress amplification in a wall, or to understand the crack path in wall.

References

[1] "CEN, Eurocode 6, Design of masonry structures, Part 1, Common rules for reinforced and unreinforced masonry structures", EN-1996-1-1, 2005.
[2] T.T. Bui, A. Limam, Discrete element modelling of the in-plane and out-of-plane behaviour of dry-joint masonry wall constructions, Eng. Struct. 136 (2017) 277–294.
[3] Gihad Mohamad, Paulo Lourenço, Humberto Roman, Mechanics of hollow concrete block masonry prisms under compression: review and prospects, Cem. Concr. Compos. 29 (2007) 181–192.
[4] Waleed Thanoon, Finite element analysis of interlocking mortarless hollow block masonry prism, Comput. Struct. 86 (2008) 520–528.
[5] Waleed Thanoon, Nonlinear finite element analysis of grouted and ungrouted hollow interlocking mortarless block masonry system, Eng. Struct. 30 (2008) 1560–1572.
[6] Gihad Mohamad, Fernando Fonseca, Vermeltfoort, Dirk Martens, Paulo Lourenço, Strength, behaviour, and failure mode of hollow concrete masonry constructed with mortars of different strengths, Const. Build. Mater. 134 (2017) 489–496.
[7] Ghoneim Fahmy, Behaviour of concrete block masonry prisms under axial compression, Can. J. Civ. Eng. 22 (5) (1995) 898–915.
[8] Uday Vyas, Venkatarama Reddy, Prediction of solid block masonry prism compressive strength using FE model, Mater. Struct. 43 (2010) 719–735.
[9] Anastasia Drougkas, Roca Molins, Numerical prediction of the behaviour, strength and elasticity of masonry in compression, Eng. Struct. 90 (2015) 25–28.
[10] Lourenco Zucchini, A micro-mechanical model for the homogenisation of masonry, Int. J. Solids Struct. 39 (2002) 3233–3255.
[11] Anthoine, Derivation of the in-plane elastic characteristics of masonry through homogenization theory, Int. J. Solid. Struct. 32 (2h) (1995) 137–163.
[12] Anthoine, Homogenisation of periodic masonry: plane stress, generalised plane strain or 3D modelling?, Commun Numer. Method. Eng. 13 (1997) 319–326.
[13] S. Bati, G. Ranocchiai, L. Rovero, A micromechanical model for linear homogenization of unit masonry, Mater. Struct. 32 (1999) 22–30.
[14] Panasenko Bakhvalov, Homogenization: Averaging Processes in Periodic Media, Kluwer Academic Publishers, Dordrecht, Netherlands, 1989.
[15] Lourenço Zucchini, Mechanics of masonry in compression: results from a homogenization approach, Comput. Struct. 85 (2007) 193–204.
[16] Salah Sarhat, Edward G. Sherwood, The prediction of compressive strength of ungrouted hollow concrete block masonry, Const. Build. Mater. 58 (2014) 111–121.
[17] D. Mc Nary, Abrams, Mechanics of masonry in compression, J. Struct. Eng. 111 (4) (1985) 857–870.
[18] Adrian Costigan, Sara Pavía, Oliver Kinnane, An experimental evaluation of prediction models for the mechanical behaviour of unreinforced, lime-mortar masonry under compression, J. Build. Eng. 4 (2015) 283–294.
[19] Shariar Agaajani, Danièle Waldmann, "Stabilité de système de murs en blocs de béton emboitable sans joints en mortier", in Regroupement francophone pour la recherche et la formation sur le béton, Lyon, France, 2012
[20] Shariar Agaajani, Development and investigation of a new dry-stacked wall system, University of Luxembourg, Thesis, 2015.
[21] K. William, E.D. Warnke, Constitutive model for the triaxial behaviour of concrete, in: Proceedings of international association of bridge and structural engineers (ISMES), Bergamo, Italy, 1975.
[22] Alwathaf Jaafar, Behaviour of interlocking mortarless block masonry, Const. Mater. 159 (2006) 111–117.
[23] B. Jonaitis, R. Zavalis, Experimental research of hollow concrete block masonry stress deformations, Conf. Mod. Build. Mater. Tech. Proc. Eng. 57 (2013) 473–478.
[24] R. Atkinson, G. Kingsley, A comparison of the behaviour of clay and concrete masonry in compression, USA-JAPAN coordinated program for Masonry Buildings Research, Report N° 1, 1985.